

Tetramethylbenzidine-TetrafluoroTCNQ (TMB-TCNQF₄): A narrow-gap semiconducting salt with room temperature relaxor ferroelectric behavior

Stefano Canossa,¹ Elena Ferrari,² Pit Sippel,³ Jonas K. H. Fischer,^{3,4} Raphael Pfattner,⁵ Ruggero Frison,⁶ Matteo Masino,² Marta Mas-Torrent,⁵ Peter Lunkenheimer,³ Concepció Rovira,⁵ and Alberto Girlando^{*2,7}

¹*EMAT, Department of Physics, University of Antwerp, 2020 Antwerp, Belgium*

²*Dipartimento di Scienze Chimiche, della Vita e della Sostenibilità Ambientale (S.C.V.S.A.) & INSTM-UdR Parma, Università di Parma, 43124 Parma, Italy*

³*Experimental Physics V, Center for Electronic Correlations and Magnetism, University of Augsburg, 86159 Augsburg, Germany*

⁴*Tohoku Forum for Creativity, Tohoku University, 980-8577 Sendai, Japan*

⁵*Department of Molecular Nanoscience and Organic Materials,*

Institut de Ciència de Materials de Barcelona (ICMAB-CSIC) and Networking Research Center on Bioengineering, Biomaterials and Nanomedicine (CIBER-BBN), ES-08193 Bellaterra, Spain

⁶*Physik-Institut, Universität Zürich, 8057 Zürich, Switzerland*

⁷*Present address: Molecular Materials Group, 43124 Parma, Italy*

We present an extension and revision of the spectroscopic and structural data of the mixed stack charge transfer (CT) crystal 3,3',5,5'-tetramethylbenzidine-tetrafluoro-tetracyanoquinodimethane (TMB-TCNQF₄), associated with new electric and dielectric measurements. Refinement of synchrotron structural data at low temperature has led to revise the previously reported [Phys. Rev. Mat. **2**, 024602 (2018)] $C2/m$ structure. The revised structure is $P2_1/m$, with two dimerized stacks per unit cell, and is consistent with the vibrational data. However, polarized Raman data in the low-frequency region also indicate that by increasing temperature above 200 K the structure presents an increasing degree of disorder mainly along the stack axis. X-ray diffraction data at room temperature have confirmed that the correct structure is $P2_1/m$ - no phase transitions - but did not allow to definitely substantiate the presence of disorder. On the other hand, dielectric measurement have evidenced a typical relaxor ferroelectric behavior already at room temperature, with a peak in real part of dielectric constant $\epsilon'(T, \nu)$ around 200 K and 0.1 Hz. The relaxor behavior is explained in terms of the presence of spin solitons separating domains of opposite polarity that yield to ferroelectric nanodomains. TMB-TCNQF₄ is confirmed to be a narrow gap band semiconductor ($E_a \sim 0.3$ eV) with room temperature conductivity of $\sim 10^{-4} \Omega^{-1} \text{ cm}^{-1}$.

I. INTRODUCTION

Over the last few years, mixed-stack (ms) organic charge-transfer (CT) crystals have attracted great interest due to their unique properties of high tunability and promising applications in several fields of organic electronics, from Organic Field Effect Transistors (OFET) [1, 2], to photovoltaic devices [3], to organic ferroelectrics [4], and so on. In the case of binary molecular systems, ms-CT crystals consist of a regular arrangement of face-to-face stacks of π -electron donor (D) and acceptor (A) molecular moieties with a defined stoichiometry. Such stacks are called mixed to distinguish them from segregated stacks of cation (D^+) or anion (A^-) radicals in other systems. The ionicity parameter ρ represents the degree of mixing between ground and excited CT state, and plays a fundamental role in the physical properties of ms-CT crystals. The most common and most studied class of 1:1 ms-CT crystals have a neutral or quasi-neutral ground state, $\rho \lesssim 0.5$. A handful have intermediate ionicity, and some of them upon lowering temperature or increasing pressure undergo a valence instability dubbed Neutral-Ionic transition [5]. Finally, the strongest electron Donor and Acceptor molecules form radical ion salts with $\rho \approx 1$, whose Madelung energy M exceeds the energy cost, $I - A$, to transfer an electron from D to A.

Mixed stack radical salts are rare, also because strong D and A molecules may prefer to crystallize as segregated stacks, as for instance DBTTF-TCNQF₄, [6] or TMPD-TCNQF₄ [7]. As a matter of fact, old literature search provided just four ionic ($\rho \geq 0.9$) ms-CT crystals, namely, TMPD-TCNQ [8], M₂P-TCNQF₄ [9], TTF-BA [10], and BEDO-TCNQCl₂ [11]. The three former all exhibit a spin Peierls transition around 200 K, 120 K and 50 K, respectively, whereas BEDO-TCNQCl₂ displays a first order transition around 100-120 K of unclear origin, but without stack dimerization.

More recently, some of us obtained another ionic ($\rho \simeq 0.9$) ms-CT crystal, TMB-TCNQF₄, whose room T vibrational spectra clearly indicate a dimerized stack, whereas for X-ray the stack appeared as regular (equal distances between D and A) [12]. We have decided to further investigate this system, also including electric and dielectric measurements. Indeed, very little is known about semiconducting properties of ionic ms-CT crystal. Furthermore, the above mentioned TTF-BA has been the first ms-CT crystal displaying ferroelectric properties in the low- T phase, where the stack is dimerized [13]. The new measurements reveal an actual dimerized stack structure already at room temperature T , with an intriguing relaxor ferroelectric behavior.

II. METHODS

A. Sample preparation

The crystals have been prepared by sublimation at about 180 °C in an open tube under controlled atmosphere [12], with a simplified version of the physical transport apparatus described by Laudise *et al.*[14].

B. Electric and dielectric measurements

Homogeneous thin single crystals of TMB-TCNQF₄ were analyzed under an optical microscope equipped with a polarizer/analyzer setup and electrostatically transferred Si/SiO₂ substrates with 200 nm thermally grown oxide thickness. Single crystals were electrically connected employing high conductive graphite paste (Dotite XC-12) and thin gold wires at the opposite tip of the needle-like crystals. Crystal dimensions were estimated using an optical microscope. Samples were prepared and electrically connected under ambient conditions (Relative humidity rH=40-60 % and temperature $T = 28^\circ\text{C}$). All electrical characterization was carried out in darkness within an nitrogen filled glove box with low humidity and oxygen levels ($\text{H}_2\text{O} < 2$ ppm, and $\text{O}_2 < 2$ ppm) using a Keithley SourceMeter model 2612. Pseudo AC measurements at low current were used to prevent Joule heating of the sample.

The dielectric constant and conductivity were determined using a frequency-response analyzer (Novocontrol Alpha-A). Gold wires were attached to contacts of gold paint on opposite tips of the needle-like crystals, ensuring an electric-field direction exactly parallel to the stack axis. Sample cooling and heating were achieved by a nitrogen-gas cryosystem (Novocontrol Quatro).

C. Spectroscopic measurements

Polarized infrared (IR) absorption spectra of the crystals were recorded with a Bruker IFS-66 Fourier transform spectrometer coupled to the Hyperion 1000 IR microscope equipped with a wire-grid polarizer. Spectral resolution: 2 cm^{-1} . The Raman spectra with 752 nm excitation (Lexel Kr laser) were recorded with a Renishaw 1000 Raman spectrometer with the appropriate edge filter and coupled to a Leica M microscope. Raman spectra with the other exciting lines were obtained with Horiba LabRAM HR Evolution spectrometer equipped either with a Ultra Low-Frequency (ULF) Bragg filter or with the appropriate edge filter. Spectral resolution 2 cm^{-1} . Incident and scattered polarization was controlled by a half-wave plate and a thin-film linear polarizer, respectively, and the sample was rotated to record the different polarizations. A small liquid nitrogen cryostat (Linkam HFS 91) was used for temperature-dependent measurements under the IR and Raman microscopes.

D. Structural measurements

Low temperature (100, 150 and 200 K) diffraction data were obtained at the XRD1 beamline of the Elettra Synchrotron facility (CNR Trieste, Italy), with beam energy of 17.712 keV. Diffraction data at 300 K were collected using a Rigaku-Oxford SuperNova diffractometer, equipped with Cu K α (8.04 keV) X-ray source. Data collection, refinement procedures and structural analysis are described in detail in the Supporting Information. The structures have been deposited at the Cambridge Crystallographic Data Center (deposition numbers CCDC 2097174-2097177) and can be obtained free of charge from the CCDC at www.ccdc.cam.ac.uk/getstructures.

III. RESULTS

A. Electric and dielectric measurements

As TMB-TCNQF₄ is a rare ionic mixed stack, we believed it was important to have a characterization of its electric and dielectric properties, by building transistors and condensers, as detailed in the Methods Section and in the Supporting Information. Two crystals, sample 1, Fig. S3 left, and sample 2, Fig. S3 right, were measured and showed high source-drain currents (I_D) in FET measurements at low drain voltages with corresponding gate-leakage currents of at least two orders of magnitude smaller. No clear field-effect was observed in the applied voltage range, in contrast to what it has been recently reported by Uekusa *et al.* [15] with a series of TMB Acceptor CT crystals and films. Crystal bulk conductivity is probably dominant in the measured current, and the contribution of a possible thin-gate induced transistor channel at the dielectric/semiconductor interface is not clearly detectable. Estimated bulk conductivity values for sample 1 and sample 2 were $\sigma_1 = 4 \cdot 10^{-4}\text{ S/cm}$ and $\sigma_2 = 2.2 \cdot 10^{-4}\text{ S/cm}$, respectively. The dc conductivity, measured at room T at low current, is around $3 \cdot 10^{-4}\text{ }\Omega^{-1}\text{ cm}^{-1}$. The T dependence of the conductance, evaluated

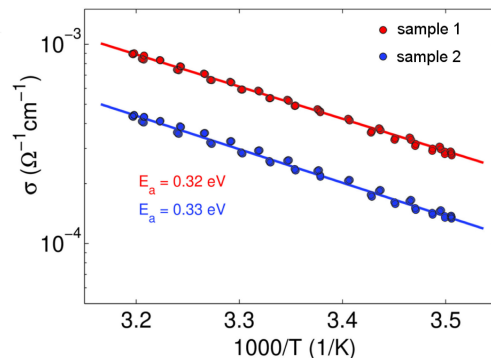


FIG. 1. Temperature dependence of the TMB-TCNQF₄ dc-conductivity obtained through transistor measurements.

as detailed in the Supporting Information, is reported for two samples in Figure 1, and allows the extraction of the activation energy E_a , which turns out to be $0.32 - 0.33$ eV, in agreement with Ref. [15].

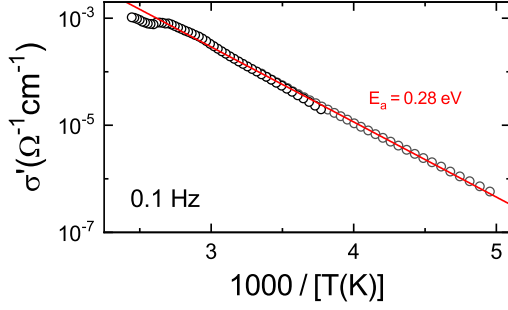


FIG. 2. Temperature dependence of the TMB-TCNQF₄ conductivity obtained by low-frequency dielectric measurements.

The temperature dependence of the conductivity can also be obtained from low-frequency dielectric measurements, as reported in Fig. 2. At such low-frequency (0.1 Hz), $\sigma'(\omega, T)$ represents an estimate of the dc conductivity. At 300 K the conductivity value is around $9 \times 10^{-5} \Omega^{-1} \text{ cm}^{-1}$, whereas the activation energy, estimated by applying the least square fitting to the linear part of the conductivity shown in Fig. 2, is 0.28 eV. In conclusion, both dc and low-frequency conductivity measurements classify TMB-TCNQF₄ crystal as a narrow-gap semiconductor ($E_a \sim 0.3$ eV), with a relatively high conductivity at room T ($\sim 10^{-4} \Omega^{-1} \text{ cm}^{-1}$).

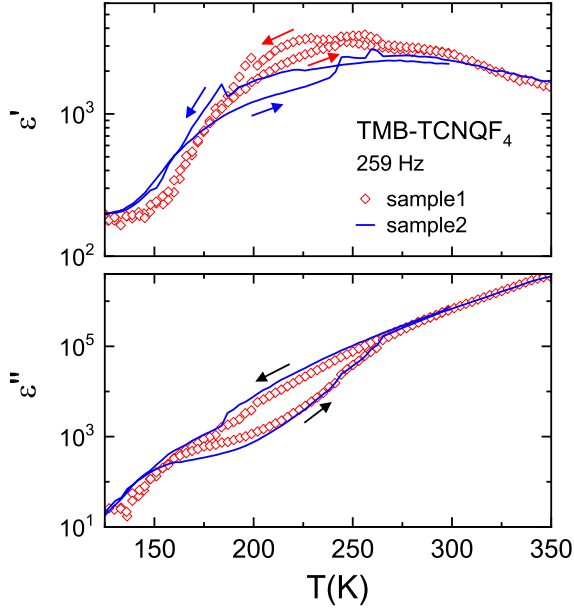


FIG. 3. Temperature dependence of the real and imaginary part of the dielectric constant of two TMB-TCNQF₄ samples at 259 Hz. The temperature cycle evidence a sort of hysteretic behavior between 270 and 170 K.

Additionally, the dielectric measurements as a function of T and frequency revealed a strange hysteretic behavior, as exemplified by the T dependence of the real (ϵ') and imaginary (ϵ'') parts of the dielectric constant at 259 Hz shown in Fig. 3. The minor anomalies observed in both quantities seem to look quite similar in two different samples, which is puzzling and speaks against a non-intrinsic origin. We do not have any evidence of a phase transition, and in any case the width of the hysteresis seems too large for it.

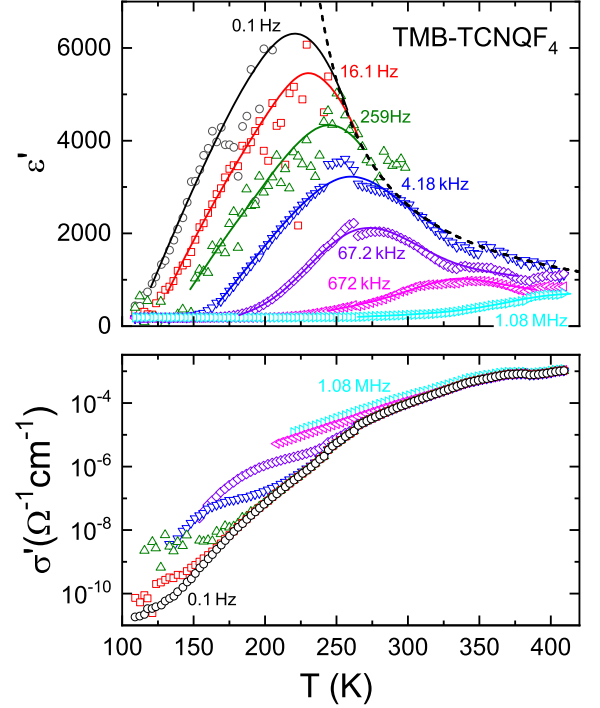


FIG. 4. Top panel: temperature dependence of the real part of the dielectric constant $\epsilon'(T)$. The solid lines are guides for the eyes. The dashed line demonstrates Curie-Weiss behavior with $T_{CW} = 202$ K. Bottom panel: temperature dependence of the frequency dependent conductivity $\sigma'(T)$.

In the top panel of Fig. 4 the temperature-dependent real part of the dielectric constant is shown for frequencies between 0.1 Hz and 1.08 MHz. We observe large peaks in the permittivity, that decrease in amplitude and shift to higher temperature with increasing frequency. This corresponds to the typical behavior of relaxor ferroelectrics [16, 17]. Due to the needle-like geometry, the electrode area and thus the measured capacitance are very small, leading to a large uncertainty in the absolute values of ϵ' . Finally, the dashed line in the top panel of Fig. 4 demonstrates that the right flanks of the relaxor peaks, representing the static dielectric constant, can be described by a Curie-Weiss law with a Curie-Weiss temperature of $T_{CW} \approx 202$ K, which provides an estimate of the quasi-static freezing temperature. The $\sigma'(T)$ plots reported in the bottom panel of Fig. 4 reveal indications of the loss peaks, expected for relaxors. Their right

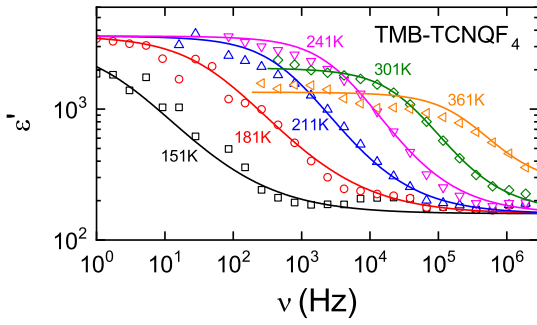


FIG. 5. Frequency-dependent plot of the dielectric constant $\epsilon'(\nu)$ of TMB-TCNQF₄ at various temperatures. Lines are fits with the Cole-Cole function.

flanks are partly superimposed by the dc conductivity, approximated by the 0.1 Hz curve (cf. Fig. 2).

Frequency-dependent plots of the dielectric constant $\epsilon'(\nu)$ are shown in Fig. 5 for various temperatures. The spectra reveal a step-like decrease of $\epsilon'(\nu)$ which shifts to lower frequencies with decreasing temperature. This evidences the slowing down of relaxational dynamics with decreasing T . Similar to the peaks in $\epsilon'(T)$, the heights of the curves in $\epsilon'(\nu)$ decrease with increasing temperature, typical of relaxor ferroelectrics [16, 17].

To further analyze the relaxor dynamics, Fig. 6 presents an Arrhenius plot of the temperature-dependent relaxation times as determined from the fits shown in Fig. 5. The linear Arrhenius fit (line in the figure) yields an activation energy $E_a \sim 0.28$ eV, and a pre-exponential factor $\tau_0 = 5.9 \times 10^{-11}$ s. Similar Arrhenius behavior we have also observed for another organic relaxor, M₂P-TCNQ [18], whereas most, but not all, relaxor ferroelectrics can be described by the Vogel-Fulcher-Tammann law [19–21]. It is interesting to note that we have determined identical energy barriers for the dipole motion and the dc charge transport, indicating a close coupling of both dynamics.

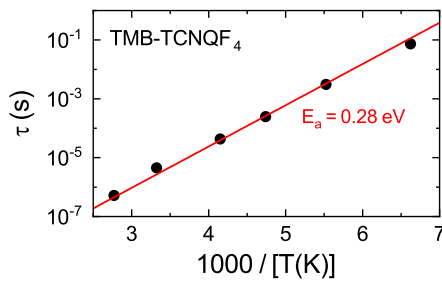


FIG. 6. Temperature evolution of TMB-TCNQF₄ relaxation time in an Arrhenius plot. The line shows an Arrhenius fit.

Before closing this Section, a word of caution is necessary. In fact, one must be aware that a non-intrinsic, contact-related origin of the found relaxation process cannot be completely excluded. The usual tests to check

for this effect, namely measurements with different sample geometries and with very different contact types cannot be easily done for the present needle-like, very brittle samples. Due to the sample geometry and the conductivity of the samples, we also cannot apply very high fields to check for hysteresis or polarization in the presumed relaxor ferroelectric state. However, the presence of (partially) ordered dipoles implied in a ferroelectric behavior is consistent with the lack of inversion center in the stack, as suggested by the reported vibrational measurements.[12]

B. Temperature dependence of the vibrational spectra and revision of the crystal structure

According to the reported crystal structure [12], at room temperature TMB-TCNQF₄ crystallizes in the monoclinic system $C2/m$ (C_{2h}^3), with two DA pairs per unit cell. All the molecules reside on inversion centers so that the stack appears to be regular. On the other hand, it has been also noted that the room temperature IR spectra polarized parallel to the stack are characterized by the presence of strong IR absorptions induced by the electron-molecular vibration (e-mv) coupling at the same frequencies of the main Raman bands [12]. This is an unquestionable hint of the loss of inversion center, i.e., the stack appears to be dimerized, in contrast to the X-ray crystal structure.

There are several other cases of inconsistency between the results of X-ray and of vibrational spectroscopy, since the former probes long-range order and the latter the local (DA pair) structure. All these discrepancies have been explained in terms of some kind of disorder, either static or dynamic [8, 22–24]. In the case of TMB-TCNQF₄, lack of inversion center and disorder at the nanoscale are also implied by the relaxor behavior illustrated in the previous Section. We have then decided to examine the temperature dependence of the vibrational spectra, to investigate if a disorder-to-order phase transition was present, like in the case of two other examples we are aware of [8, 23].

With IR spectroscopy, we could go both above and below room temperature, as exemplified in Figure 7. No visually appreciable band intensity variations are detected between 380 and 80 K. To confirm this finding, we measured the relative intensity of four e-mv induced bands (marked in the top panel of the Figure as a black circle, a red square, a magenta diamond and a blue triangle) with respect to a normally IR active band detected in the spectrum polarized perpendicularly to the stack (marked by an asterisk in the bottom panel of the Figure). The results are plotted in the inset of Figure 7. The average relative intensity shows a slight increase in going below about 220 K, but the change is well within the estimated error bars, which are larger at high T since the bands become broader. Therefore there is no clear-cut evidence of a disorder-to-order transition by lowering T , but rather a behavior similar to that observed for the temperature

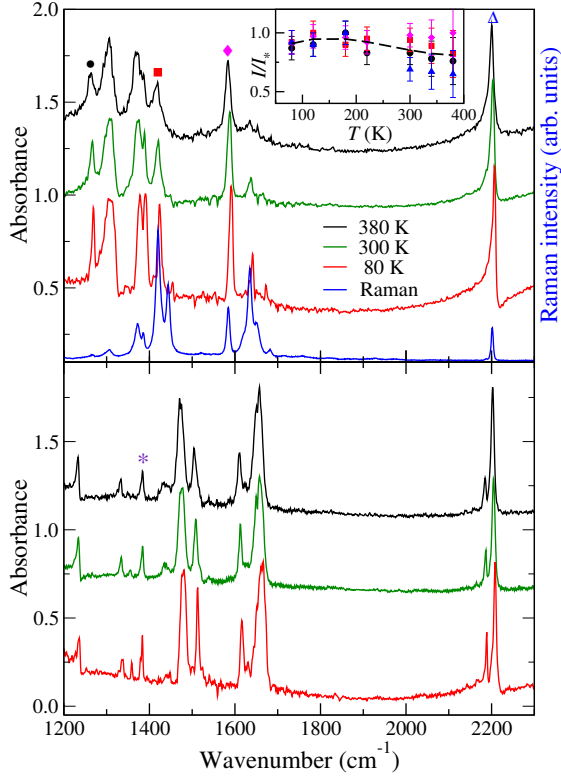


FIG. 7. Infrared spectra of TMB-TCNQF₄ as a function of T . Top panel: Spectra polarized parallel to the stack axis, compared with the 300 K Raman one (blue) to evidence the vibronic bands. Bottom panel: Spectra polarized perpendicular to the stack axis. Inset of top panel: T evolution of the ratio of the intensity of four e-mv induced bands (marked as black dot, red square, magenta diamond and blue triangle) with respect to a normally infrared active band (marked by an asterisk in the bottom panel).

dependence of the dielectric constant (Figure 3).

Raman spectroscopy in the low-frequency (10–200 cm^{-1}) region, involving lattice phonons, is known to be very sensitive to molecular packing [25] and also to disorder in a scale of a few unit cells [26], hence intermediate between the long-range order of X-ray and the local structure probed by high-frequency, intramolecular vibrations. We have thus obtained the low-frequency polarized Raman spectra of TMB-TCNQF₄ as a function of temperature shown in Figure 8.

The selection rules for TMB-TCNQF₄ Raman active lattice phonons in terms of the $C2/m$ (C_{2h}^3) factor group and adopting the rigid molecule approximations [27], are as follows: $2 A_g + 4 B_g$. So we expect only six bands, corresponding to the librations of the molecules, since the primitive cell contains just one DA pair, with each molecule on inversion center. A look at the experimental spectra shows that these spectral predictions are not obeyed, as there are more bands than expected. The highest frequencies bands, above 160 cm^{-1} , might also involve the methyl rotations, but even without counting them we observe eight bands, which become 10 at 80 K

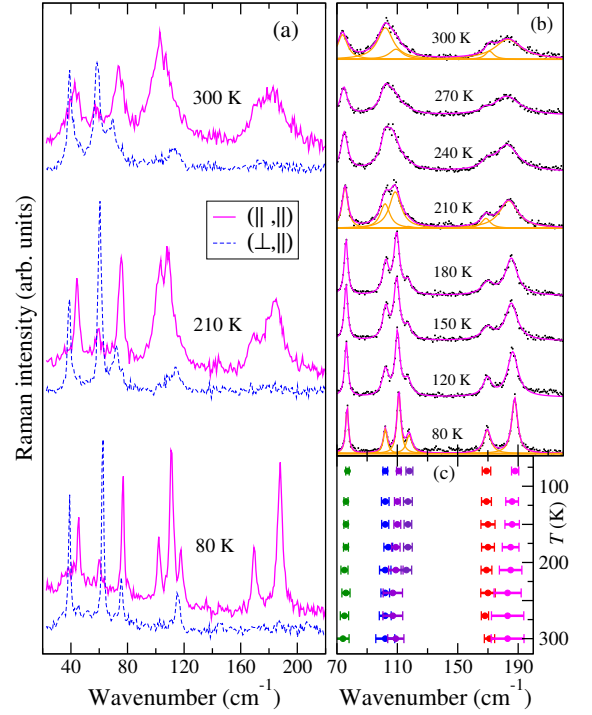


FIG. 8. Low-frequency Raman spectra as a function of temperature. (a) Spectra at three significant temperatures. The \parallel and \perp symbols within parenthesis indicate the polarization of incident and scattered light with respect to the stack axis. (b) Full T evolution of an enlarged portion of the (\parallel, \parallel) spectra. Black dots represent the experimental spectra, magenta lines the fitting with a set of Lorentzian functions. The single Lorentzians are reported as orange lines for the three most significant temperatures. (c) T evolution of the peak frequencies (dots) and of the corresponding FWHM (full width at half maximum, here represented as error bars) of the bands of panel (b).

(Panel (a) of Fig. 8). Therefore the lattice mode spectral region, like that of the intramolecular vibrations, tells us that the previously reported space group [12] is not the correct one.

In addition, at room temperature the spectra recorded with incident and scattered light polarized along the stack, labeled (\parallel, \parallel) , show two rather broad bands around 100 and 180 cm^{-1} , which by lowering T narrow and separate in more components, as detailed in panel (b) of the Figure. Notice also that the bandwidths observed in the other polarization are normal. This situation is reminiscent of what it has been observed in another CT crystal, [18]. In that case, the band broadening has been attributed to the electron-phonon coupling, since the broad bands also exhibit a marked frequency hardening by increasing the temperature, and their intensity is strongly enhanced by moving the frequency of the Raman exciting line towards the far-red, going into pre-resonance with the CT transition. Strong electron-phonon coupling means strong phonon anharmonicity, hence the line broadening.

To test if this explanation is valid also for TMB-TCNQF₄, we have followed in detail the temperature evolution of Raman bands in the (\parallel , \parallel) polarization, by performing a deconvolution in terms of Lorentzians, as exemplified for three temperatures by the orange lines in panel (b). Panel (c) summarizes such an analysis, in terms of the peak frequencies and Lorentzian FWHM, the latter represented by error bars. It is seen that the above-mentioned two groups of bands around 100 and 180 cm⁻¹ start to separate around 200 K, but no anomalous frequency hardening is evident by lowering the temperature. Furthermore, the spectra recorded by moving the exciting line toward the CT transition (see Supporting Information, Figures S1 and S2) show an intensity enhancement much less pronounced than in the case of M₂P-TCNQ [18]. Therefore in this case the remarkable band broadening and line merging observed by going towards room temperature cannot be fully ascribed to the effect of electron-phonon coupling. In other words, whereas the anomalous band broadening observed in M₂P-TCNQ is mostly due to phonon anharmonicity, and can be assimilated to the so-called dynamic or thermal disorder, the analogous broadening we observe in TMB-TCNQF₄ must have a different origin. We believe it is due to disorder in the lattice structure along the stack axis, namely, to static, or displacement, disorder [28].

In summary, low-frequency Raman spectroscopy, like IR, tells us that the space group symmetry is *lower* than that obtained in the standard refinement of the room temperature X-ray data [12], and that above ≈ 200 K there is some kind of disorder along the stack.

In order to clarify the apparent discrepancy of X-ray with respect to vibrational and dielectric measurements, we used synchrotron radiation for a new structural analysis, carefully inspecting the reciprocal space of the samples to look for signs of diffuse scattering, of phase transitions, or of altered symmetry. This set of measurements was limited to cryogenic conditions (100, 150 and 200 K), to avoid the risk of beam damage.

Overall, no significant diffuse scattering features were found, which could agree with correlated disorder along the molecular stacking direction, while a strong crystal mosaicity elongates all reflections, hampering a reliable diffuse scattering analysis. However, the presence of strong reflections violating a C centering of the unit cell (cf. Figure S7) proved that the symmetry is indeed lower than the previously reported one [12]. Successful indexing of all reflections was achieved with space group $P2_1/m$ rather than $C2/m$ [12], while maintaining the same unit cell metric and orientation. Full details of the new crystallographic analysis can be found in the Supporting Information.

The $P2_1/m$ structure features two stacks (two formula units) per unit cell, aligned along the a axis (Figure 9). Most importantly, and differently from what was modeled by using $C2/m$ space group, these stacks are dimerized, and the inversion center is *between* the stacks.

Therefore the two DA dimers in the unit cell have anti-ferroelectric arrangement. The intra-dimer and inter-dimer distances along the stack at 100 K are 3.1447(10) and 3.4415(11), so that the dimerization amplitude $\delta = (d_2 - d_1)/(d_2 + d_1)$ is 0.05 (Figure S5), about twice that of the of the prototypical CT crystal Tetrathiafulvalene-Chloranil (TTF-CA) in the low temperature phase [29]. The crystal structure also evidences the presence of a network of hydrogen bonds between the methyl and the cyanide groups (Figure 9 (b)). These cooperate with the CT stacking interactions, while more directional H-bonds contacts are found between cyanide and amino groups of molecules belonging to different stacking columns (Figure 9 (c)). All these intermolecular interactions can also be visualized in terms of the Hirshfeld surfaces provided by the program Crystal Explorer 17 [30], as detailed in the Supporting Information.

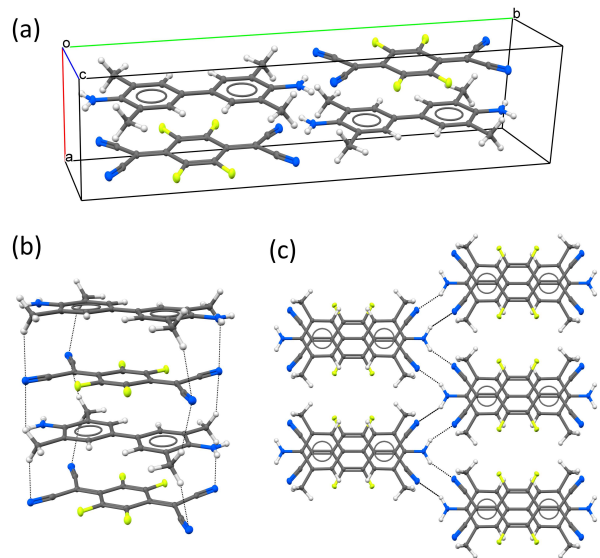


FIG. 9. Structure of TMB-TCNQF₄ at 100 K. The main intra- and inter-stack hydrogen bonding between TMB and TCNQF₄ are shown in (b) and (c), respectively.

The number of bands observed in the low-frequency Raman spectra (Figure 8) is consistent with the revised $P2_1/m$ structure, as are the e-mv induced bands observed in IR (Figure 7), since the primitive cell contains two dimerized stacks. We have collected a new set of X-ray data at 300 K, verifying that structure remains the same also at room temperature. Indeed, the weak extra peaks due to the primitive $P2_1/m$ lattice are also present in the room temperature X-ray diffraction patterns (Figure S7), and these were ignored in the previous automatic structure refinement.[12] Therefore there are no phase transitions up to 300 K. However, the new temperature dependent structural analysis suggests that something is happening between 300 and 200 K. For instance, the dimerization amplitude δ increases from 0.04 to 0.05 by lowering T in this interval, then it remains

practically constant down to 100 K (Figure S5), a behavior consistent with the increase of the intensity of the e-mv induced bands (inset of Figure 7). Relaxor behavior and the low-frequency Raman spectra suggest the presence of some kind of disorder above ≈ 200 K.

We attempted an analysis of the temperature dependence of the anisotropic displacement parameters, ADP [31]. The ADP T dependence gives some hint of disorder along the stack above 200 K, but the fact that we do not have structural data between 200 and 300 K, and that the 300 K data have been collected with a different technique and on a different sample with respect to the others, prevent us to conclude anything definitive. Indeed, the investigation of the disorder by structural methods, for instance by pair-distribution function analysis, would require temperature dependent synchrotron radiation or neutron diffraction (in view of the above evidenced importance of hydrogen bonding) on a unique crystal having optimal crystallinity, and from ambient conditions to 100 K in finer steps. Such deep investigation is certainly desirable, as it would allow a direct and hopefully precise connection with vibrational and dielectric measurements, but goes well beyond the scope of the present work.

IV. DISCUSSION AND CONCLUSIONS

The measurements presented here show that the physics of TMB-TCNQF₄ is quite interesting and peculiar, but also rather complex, so that its understanding still requires additional experiments aimed to provide suitable data for a better modeling. It has been shown that TMB-TCNQF₄ is a narrow gap semiconductor ($E_a \simeq 0.3$ eV), with an optical gap of about 0.8 eV, and a quasi ionic ground state ($\rho \simeq 0.9$) [12]. The most important advancements of the present study with respect to the previous ones [12, 15] consist in the finding that TMB-TCNQF₄ stacks are dimerized, and that some kind of disorder along the stacks is likely present above ≈ 200 K, a fact that is also reflected by the observed relaxor behavior. As it is generally the case with relaxors, [32] the passage from the disordered to the ordered structure takes a large T interval, ≈ 100 K (Figs. 3, 7, and 8), and does not look like a real phase transition. Moreover, we have found that the room T conductivity is relatively high ($\sim 10^{-4} \Omega^{-1} \text{ cm}^{-1}$), and decreases by three orders of magnitude in going to 200 K. Finally, relaxor-ferroelectric-like behavior has been observed already at room temperature, with a maximum in $\epsilon'(\nu, T)$ around 200 K and 0.1 Hz (top panel of Fig. 4). The relaxor behavior is consistent with the disorder, but not with the anti-ferroelectric arrangements of the two stacks in the unit cell.

Modeling of TMB-TCNQF₄ physical properties in terms of a Peierls-Hubbard model and/or band structure relevant to a regular, ordered stack is clearly inappropriate [12, 15]. Electrical properties have to take into account the gap opening due to dimerization and

the effect of disorder. Simple band structure calculations (Supporting Information) for the 100 K ordered structure show that the gap is due to dimerization and not to electron-electron interactions, so TMB-TCNQF₄ has to be considered a *band*, not Mott, semiconductor. Further, deeper analyses are needed to understand the role of disorder above 200 K.

However, at the present stage we can envision a quite plausible scenario able to reconcile all the presently available experimental data, giving directions for future investigations. Analysis of the low T structures of TMB-TCNQF₄ has shown that the system is strongly 1D, with the TMB and TCNQF₄ molecules perfectly aligned on top of each other along the stacks, and weak inter-stack interactions. In going above ≈ 200 K, the structure becomes disordered *along* the stack, as indicated by the low-frequency Raman spectra and consistent with the relaxor behavior. This kind of disorder is most likely displacive, and adds to the usual thermal disorder.

As we stated in the Introduction, 1D systems like the present one are subject to the spin-Peierls instability, which is the driving force of the dimerization. However, it is also well known that in strictly 1D systems phase transitions are not allowed down to 0 K, and that fluctuations are present until 3D interactions become significant [33]. In TMB-TCNQF₄ the dimerization is probably also affected by the methyl-nitrogen contacts, (see Figure 9) but here we are proposing a rather simplified general scenario. Fluctuations involve “defects” of dimerization, boundaries between domains of different orientation, namely the spin solitons depicted in Fig. 10. At room T the disorder is likely due to presence of nanoscopic domains, which are able to move under the effect of the electric field. And there is no correlation between domains in different chains, so that we have the possibility of ferroelectric regions (indicated in pale yellow in the Figure) inside an anti-ferroelectric structure. In this model, these ferroelectric nanodomains are the origin of the relaxor behavior, in accord with the common explanation of relaxor ferroelectricity by nanoscale ferroelectric order [16, 17]. By lowering T , the population of solitons decreases, namely, the dimension of ferroelectric domains increases and their motions under the electric field becomes slower and slower until the electrostatic interactions and inter-chain hydrogen-nitrogen contacts lock the chains into the fully ordered anti-ferroelectric $P2_1/m$ structure.

Besides polyacetylene [34], spin solitons have been detected and widely studied in the CT crystal TTF-CA and derivatives in their low temperature or high pressure (p) dimerized stack phase [35–37]. Although the present data do not fully prove it, the above scenario is then quite plausible, suggesting a wide playground of new experiments and theory, perhaps more promising than that of TTF-CA. In fact, whereas in TTF-CA the studies have to be performed at low T or high p , here solitons are possibly present at ambient conditions. Since TMB-TCNQF₄ is quasi-ionic, triplet spin excitations are likely

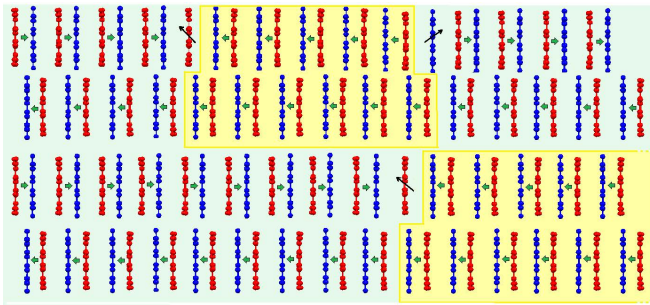


FIG. 10. Illustration of how the presence of spin solitons in TMB-TCNQF₄ yields ferroelectric domains (pale yellow regions) inside a otherwise anti-ferroelectric arrangement (light green regions). Blue molecules: TMB; red molecules: TCNQF₄. The dimerization is amplified for clarity. The green bold arrows indicate the direction of the electric dipole within the dimer, whereas the spin soliton is indicated by an inclined black arrow on the molecule.

thermally populated and easily experimentally accessible. Proper characterization of the disorder, for instance by neutron diffraction, would allow establishing the correlation length, or dimensions of the differently oriented nanodomains, which would provide the basis for a better understanding of the still rather mysterious relaxor ferroelectric behavior. Efforts should be also devoted to the growth of the crystals by different methods, possibly in the form of thin films. If successful, TMB-TCNQF₄ might be interesting even from the perspective of materi-

als application. In fact, the dimerized phase of TTF-CA has a ferroelectric arrangement, and poling yields to an ordered phase with ferroelectric hysteresis [38]. In TMB-TCNQF₄ the ordered state is anti-ferroelectric, but the ferroelectric domains would offer the possibility of building a room T relaxor ferroelectric [32].

ACKNOWLEDGMENTS

AG thanks Prof. Pascale Foury-Leylekan for very helpful discussions about the crystallographic issues. RF thanks Prof. Anthony Linden for his help in the X-ray diffraction data collection. JKHF and PL acknowledge funding from the Deutsche Forschungsgemeinschaft (DFG) via the Transregional Collaborative Research Center TRR80 (Augsburg, Munich). R.P. and M.M-T. acknowledge support from the Marie Curie Cofund, Beatriu de Pinós Fellowships (Grant Nos. AGAUR 2017 BP 00064). This work was also supported by the Spanish Ministry project GENESIS PID2019-111682RB-I00, the “Severo Ochoa” Programme for Centers of Excellence in R&D (FUNFUTURE, CEX2019-000917-S) and the Generalitat de Catalunya (2017-SGR-918). The Elettra Synchrotron (CNR Trieste) is acknowledged for granting the beamtime at the single-crystal diffraction beamline XRD1 (Proposal ID 20185483). In Parma the work has benefited from the equipment and support of the COMP-HUB Initiative, funded by the “Departments of Excellence” program of the Italian Ministry for Education, University and Research (MIUR, 2018-2022).

-
- [1] J. Zhang, J. Jin, H. Xu, Q. Zhang, and W. Huang, *J. Mater. Chem. C* **6**, 3485 (2018).
 - [2] T. Salzillo, A. Campos, and M. Mas-Torrent, *J. Mater. Chem. C* **7**, 10257 (2019).
 - [3] S. J. Kang, S. Ahn, J. B. Kim, C. Schenck, A. M. Hiszpanski, S. Oh, T. Schiros, Y.-L. Loo, and C. Nuckolls, *J. Am. Chem. Soc.* **135**, 2207 (2013).
 - [4] S. Horiuchi, K. Kobayashi, R. Kumai, and S. Ishibashi, *Chem. Lett.* **43**, 26 (2014).
 - [5] M. Masino, N. Castagnetti, and A. Girlando, *Crystals* **7**, 108 (2017).
 - [6] T. J. Emge, W. A. Bryden, F. M. Wiygul, D. O. Cowan, T. J. Kistenmacher, and A. N. Bloch, *J. Chem. Phys.* **77**, 3188 (1982).
 - [7] M. Meneghetti, R. Bozio, C. Bellitto, and C. Pecile, *J. Chem. Phys.* **89**, 2704 (1988).
 - [8] A. Girlando, A. Painelli, and C. Pecile, *Mol. Cryst. Liq. Cryst.* **112**, 325 (1984).
 - [9] M. Meneghetti, A. Girlando, and C. Pecile, *J. Chem. Phys.* **83**, 3134 (1985).
 - [10] A. Girlando, C. Pecile, and J. Torrance, *Solid State Commun.* **54**, 753 (1985).
 - [11] T. Hasegawa, T. Mochida, R. Kondo, S. Kagoshima, Y. Iwasa, T. Akutagawa, T. Nakamura, and G. Saito, *Phys. Rev. B* **62**, 10059 (2000).
 - [12] N. Castagnetti, M. Masino, C. Rizzoli, A. Girlando, and C. Rovira, *Phys. Rev. Mater.* **2**, 024602 (2018).
 - [13] F. Kagawa, S. Horiuchi, M. Tokunaga, J. Fujioka, and Y. Tokura, *Nat. Phys.* **6**, 169 (2010).
 - [14] R. Laudise, C. Kloc, P. Simpkins, and T. Siegrist, *J. Cryst. Growth* **187**, 449 (1998).
 - [15] T. Uekusa, R. Sato, D. Yoo, T. Kawamoto, and T. Mori, *ACS Applied Mater. Interfaces* **12**, 24174 (2020).
 - [16] L. E. Cross, *Ferroelectrics* **76**, 241 (1987).
 - [17] G. A. Samara, *J. Phys.: Condens. Matter* **15**, R367 (2003).
 - [18] J. K. H. Fischer, G. D’Avino, M. Masino, F. Mezzadri, P. Lunkenheimer, Z. G. Soos, and A. Girlando, *Phys. Rev. B* **103**, 115104 (2021).
 - [19] H. Vogel, *Z. Phys.* **22**, 645 (1921).
 - [20] G. S. Fulcher, *J. Am. Ceram. Soc.* **8**, 339 (1925).
 - [21] G. Tammann, *Ann. Phys. (Berlin, Ger.)* **307**, 1 (1900).
 - [22] A. Girlando, A. Painelli, and C. Pecile, *J. Chem. Phys.* **89**, 494 (1988).
 - [23] S. A. Bewick, R. A. Pascal, D. M. Ho, Z. G. Soos, M. Masino, and A. Girlando, *J. Chem. Phys.* **122**, 024710 (2005).
 - [24] M. Kumar, B. J. Topham, R. Yu, Q. B. D. Ha, and Z. G. Soos, *J. Chem. Phys.* **134**, 234304 (2011).

- [25] A. Brillante, I. Bilotti, R. G. D. Valle, E. Venuti, and A. Girlando, *CrystEngComm* **10**, 937 (2008).
- [26] A. Brillante, I. Bilotti, R. G. Della Valle, E. Venuti, A. Girlando, M. Masino, F. Liscio, S. Milita, C. Albonetti, P. D'Angelo, A. Shehu, and F. Biscarini, *Phys. Rev. B: Condens. Matter Mater. Phys.* **85**, 195308 (2012).
- [27] G. Turrell, *Infrared and Raman Spectra of Crystals* (Academic Press, 1972) Chap. 4-6.
- [28] A. Guinier, *X-Ray Diffraction* (W.H. Freeman and Co., San Francisco and London, 1963) Chap. 6.
- [29] M. Le Cointe, M. H. Lemée-Cailleau, H. Cailleau, B. Toudic, L. Toupet, G. Heger, F. Moussa, P. Schweiss, K. H. Kraft, and N. Karl, *Phys. Rev. B* **51**, 3374 (1995).
- [30] P. R. Spackman, M. J. Turner, J. J. McKinnon, S. K. Wolff, D. J. Grimwood, D. Jayatilaka, and M. A. Spackman, *J. Applied Crystallog.* **54**, 1006 (2021).
- [31] H. B. Bürgi and S. C. Capelli, *Acta Crystallogr., Sect. A: Found. Crystallogr.* **56**, 403 (2000).
- [32] C. W. Ahn, C.-H. Hong, B.-Y. Choi, H.-P. Kim, H.-S. Han, Y. Hwang, W. Jo, K. Wang, J.-F. Li, J.-S. Lee, and I. W. Kim, *J. Korean Phys. Soc.* **68**, 1481 (2016).
- [33] P. Pincus, Basic principles and concepts in the physics of low dimensional cooperative systems, in *Low-Dimensional Cooperative Phenomena*, NATO ASI B, Vol. 7, edited by H. J. Keller (Springer US, 1975) Chap. 1.
- [34] A. J. Heeger, S. Kivelson, J. R. Schrieffer, and W. P. Su, *Rev. Mod. Phys.* **60**, 781 (1988).
- [35] F. Kagawa, S. Horiuchi, H. Matsui, R. Kumai, Y. Onose, T. Hasegawa, and Y. Tokura, *Phys. Rev. Lett.* **104**, 227602 (2010).
- [36] K. Sunami, T. Nishikawa, K. Miyagawa, S. Horiuchi, R. Kato, T. Miyamoto, H. Okamoto, and K. Kanoda, *Sci. Adv.* **4**, eaau7725 (2018).
- [37] Z. G. Soos and A. Painelli, *Phys. Rev. B* **75**, 155119 (2007).
- [38] K. Kobayashi, S. Horiuchi, R. Kumai, F. Kagawa, Y. Murakami, and Y. Tokura, *Phys. Rev. Lett.* **108**, 237601 (2012).

SUPPORTING INFORMATION

Tetramethylbenzidine-TetrafluoroTCNQ (TMB-TCNQF₄): A Narrow-Gap Semiconducting Salt with Room Temperature Relaxor Ferroelectric Behavior

Stefano Canossa,¹ Elena Ferrari,² Pit Sippel,³ Jonas K. H. Fischer,^{3,4} Raphael Pfattner,⁵ Ruggero Frison,⁶
Matteo Masino,² Marta Mas-Torrent,⁵ Peter Lunkenheimer,³ Concepció Rovira,⁵ and Alberto Girlando^{*2,7}

¹ EMAT, Department of Physics, University of Antwerp, 2020 Antwerp, Belgium

² Dipartimento di Scienze Chimiche, della Vita e della Sostenibilità Ambientale (S.C.V.S.A.) & INSTM-UdR Parma, Università di Parma, 43124 Parma, Italy

³ Experimental Physics V, Center for Electronic Correlations and Magnetism, University of Augsburg, 86159 Augsburg, Germany

⁴ Tohoku Forum for Creativity, Tohoku University, 980-8577 Sendai, Japan

⁵ Department of Molecular Nanoscience and Organic Materials, Institut de Ciència de Materials de Barcelona (ICMAB-CSIC) and Networking Research Center on Bioengineering, Biomaterials and Nanomedicine (CIBER-BBN), ES-08193 Bellaterra, Spain

⁶ Physik-Institut, Universität Zürich, 8057 Zürich, Switzerland

⁷ Present address: Molecular Materials Group, 43124 Parma, Italy

Contents

- 1. Raman spectra with different exciting lines**
- 2. FET measurements**
- 3. Pseudo AC conductivity measurements**
- 4. Crystallographic structure information**
- 5. Band structure calculations**
- 6. References**

1. Raman spectra with different exciting lines

Room temperature polarized Raman spectra were collected with different excitation lines (from 633 to 1064 nm) to investigate the intensity enhancement in approaching the CT transition, located at 6500 cm^{-1} (0.81 eV) [1]. Figure S1 shows that in the (\parallel,\parallel) polarization (red lines) the low-frequency modes are clearly enhanced with respect to the intra-molecular modes and low-frequency modes in the (\perp,\perp) polarization (blue lines). However, this resonance effect is considerably lower than that observed in the previously studied dimerized stack CT crystal $\text{M}_2\text{P-TCNQ}$ [2].

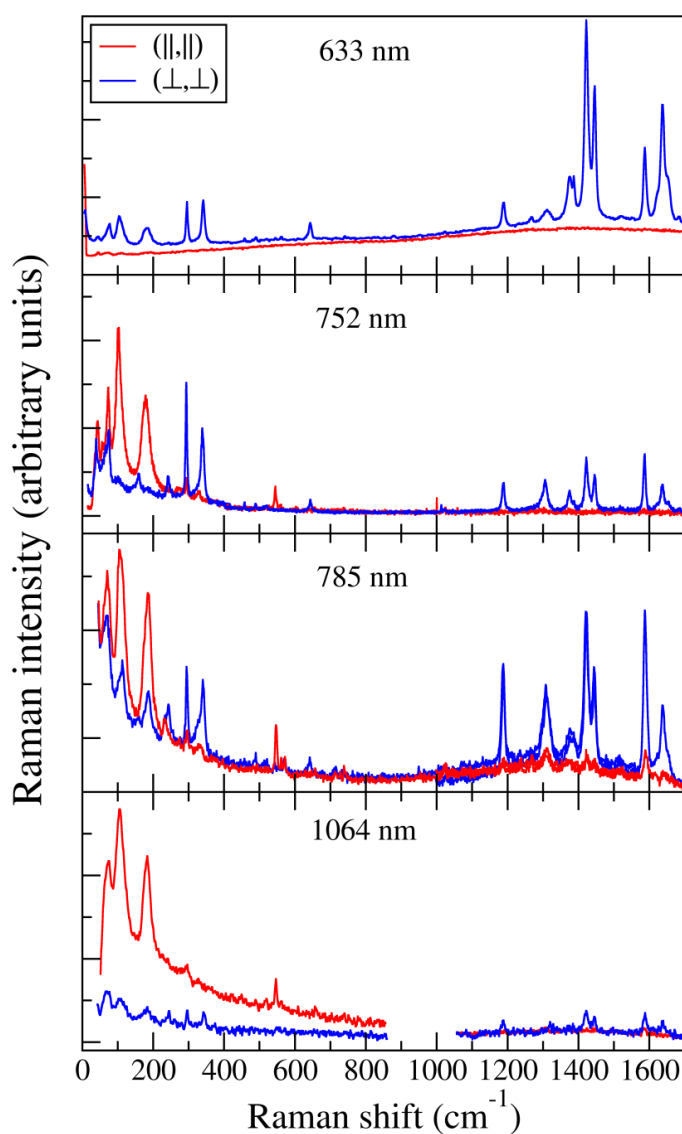


Figure S1. Polarized Raman spectra of TMB-TCNQF_4 as a function of the laser exciting line. Red lines: Incident and scattered radiation polarized parallel to the stack axis; Blue line: Incident and scattered radiation polarized perpendicular to the stack axis.

In order to better justify the above assertion, in Figure S2 we have plotted for both compounds the intensity of one low-frequency mode in the (\parallel,\parallel) polarization with respect to the intensity of a nearby mode in the (\perp,\perp) polarization, which is not affected by resonance with the CT transition. It is seen that with excitation in the red (~ 1.6 eV) the enhancement for M_2P -TCNQ is about five times as large as that of TMB -TCNQF₄, although the excitation line is more close to the CT transition energy (dotted lines in the left of the Figure).

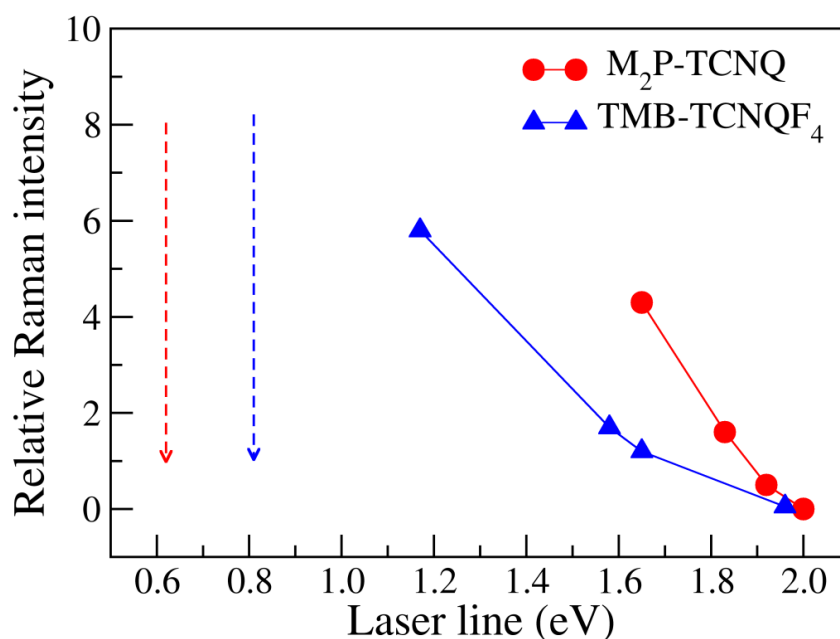


Figure S2. Blue triangles: Relative Raman intensity of the TMB -TCNQF₄ 103 cm^{-1} band in the (\parallel,\parallel) polarization with respect to the 292 cm^{-1} one in the (\perp,\perp) polarization, as a function of the laser exciting line (expressed in eV). Red circles: Relative Raman intensity of the M_2P -TCNQ 125 cm^{-1} band in the (\parallel,\parallel) polarization with respect to the 320 cm^{-1} one in the (\perp,\perp) polarization [2]. The vertical blue and red dotted lines on the left indicate the CT frequency of the two crystals.

2. FET measurements

Figures S3 show the FET output characteristics measured for two single crystals of TMB-TCNQF₄ namely sample 1 and sample 2.

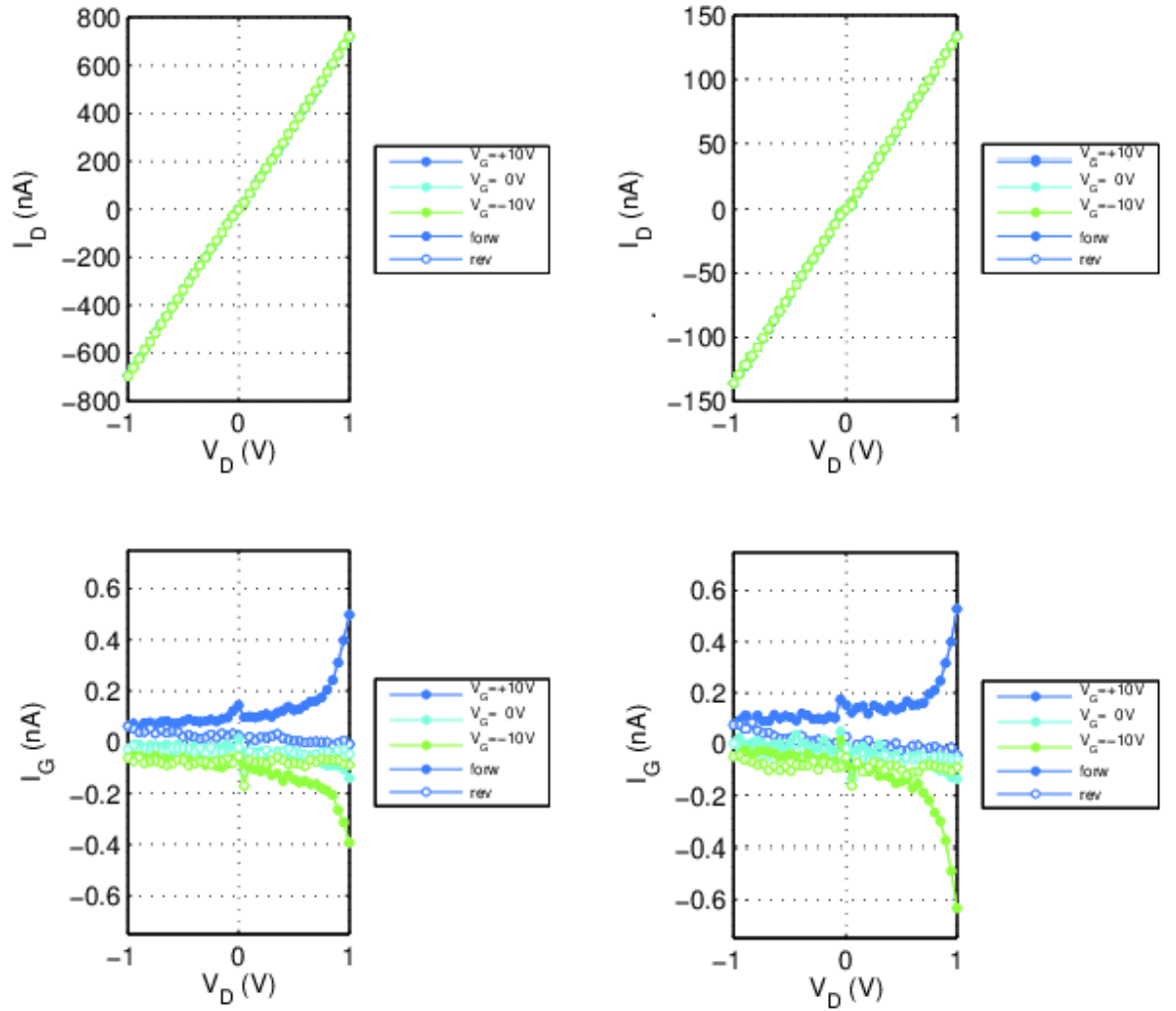


Figure S3. Field-Effect transistor output characteristics ($I_D(V_D)$) of sample 1 (left) and sample 2 (right) including leakage currents ($I_G(V_D)$) both in forward and reverse drain voltage sweeps.

3. Pseudo AC conductivity measurements

To extract the temperature dependence of TMB-TCNQF₄ single crystals, the substrates were mounted to an aluminum frame equipped with a Peltier element. Temperature was monitored in real-time using a calibrated Pt₁₀₀₀ sensor. First and second order temperature resistance coefficients were extracted for both crystals using Equation 1 exhibiting $\alpha = -9.13$ (%/K) and $\beta = 0.10$ (%/K²), respectively, as illustrated in Figure S4.

$$R(T) = R_{T_0} \cdot [1 + \alpha(T - T_0) + \beta(T - T_0)^2] \quad (1)$$

The activation energy was extracted using Equation 2, giving values of $E_a = 0.32$ eV and $E_a = 0.33$ eV, for sample 1 and sample 2, respectively.

$$\sigma = \sigma_0 \cdot \exp(-E_a / k_B T) \quad (2)$$

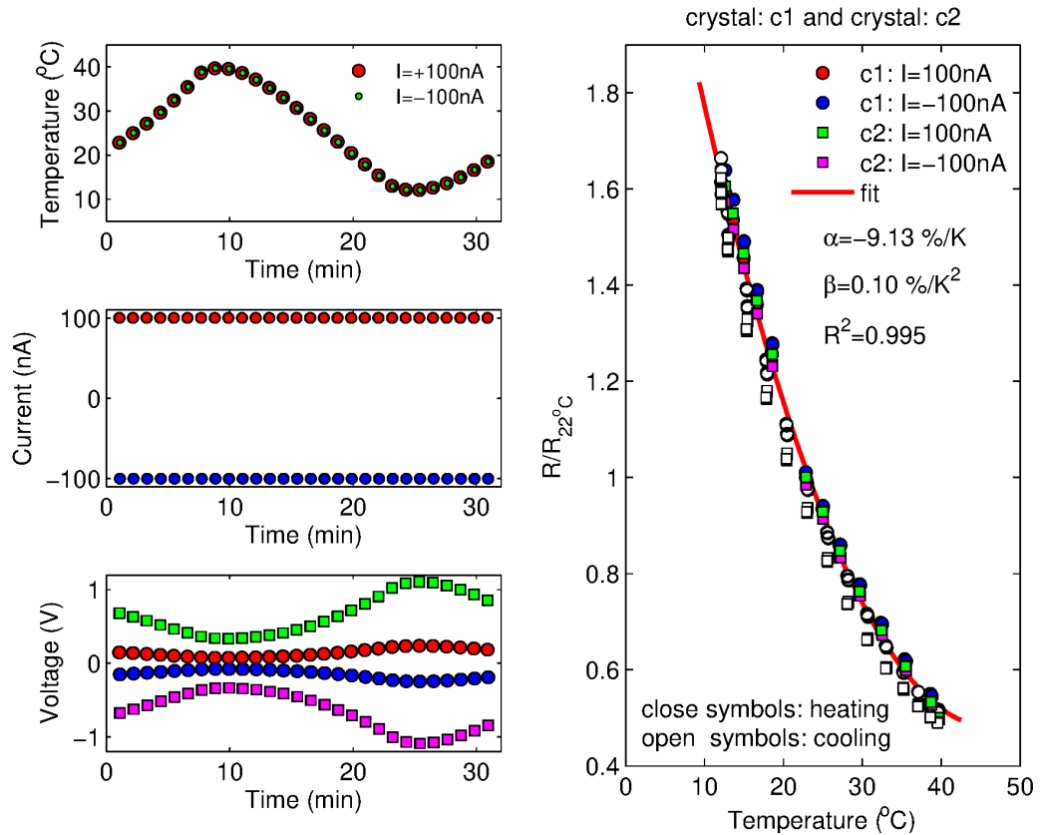


Figure S4. Temperature dependence of two TMB-TCNQF₄ crystals employing pseudo AC current of $I = \pm 100$ nA while measuring two probe resistance. a) Temperature ramp starting at room temperature heating up to $T=40$ °C followed by cooling ramp down to $T=10$ °C and back to room temperature. b) Applied current values to both crystals and c) measured voltage values. d) Calculated electrical resistance ($R/R_{22^\circ\text{C}}$) as function of temperature for both crystals including heating (closed symbols) and cooling (open symbols) cycles. Red curve fit for the extraction of first and second order temperature coefficients, α and β , respectively.

4. Crystallographic structure information

Diffraction data of TMB-TCQNF₄ at 100 K, 150 K and 200 K were acquired at the XRD1 beamline of the Elettra Synchrotron facility (CNR Trieste, Italy). The data acquisition strategy consisted of a Phi scan with oscillation step 0.5° and total coverage 360°. A beam energy of 17.712 KeV (0.7 Å) was used for all datasets, and the diffracted beams were collected on a Pilatus 2M hybrid photon counting detector while the temperature was maintained constant at the desired value by using a nitrogen stream produced with an Oxford Cryostream 700 (Oxford Cryosystems Ltd., Oxford, United Kingdom).

Diffraction data at 300K were collected using a Rigaku-Oxford Diffraction SuperNova diffractometer equipped with Kappa-axis four-circle goniometer, Atlas electronic CCD area detector, and Cu K α X-ray source. Diffraction patterns were acquired using a series of omega scans at different kappa and Phi angles, with angular step 1°, following an automated data collection strategy optimization computed by the software controlling the instrument.

Diffraction datasets have been processed using the Rigaku CrysAlisPro version 1.171.38.43 software (Rigaku Corporation, Oxford, United Kingdom), which was also used for the reconstruction of the reciprocal space and precession images (resolution 0.8 Å, inversion symmetry used).

Structure analysis was conducted by using the software Olex2 [4], using the programs ShelXT [5] and olex2.refine (Levenberg-Marquardt algorithm) for structure solution and refinement respectively. All atoms except hydrogens were refined anisotropically, while the latter were fixed in computed positions using the shelx commands AFIX 93, 137 and 43 for aminic, aliphatic and aromatic hydrogens respectively.

Hirschfeld surface and interactions plots were calculated by using the program Crystal Explorer v.17.5 [6], using default settings and specifying charge +1 and -1 for TMB and TCQNF₄ respectively, and spin multiplicity 2 for both.

The structures reported in this work can be accessed free of charge from the Cambridge Structural Database website (<https://www.ccdc.cam.ac.uk/structures/>); deposition numbers 2097174-2097177.

Crystal data and structure refinement for TMB-TCQNF₄ at 100K

Identification code	2097174		
Empirical formula	C ₂₈ H ₂₀ F ₄ N ₆		
Formula weight	516.505		
Temperature/K	100		
Crystal system	monoclinic		
Space group	P2 ₁ /m		
a/Å	6.58484(14)	b/Å	22.9103(5)
α /°	90	β /°	109.278(2)
Volume/Å ³	1183.36(5),	Z=2	c/Å 8.31003(18)
ρ calc/g cm ⁻³	1.450		γ /° 90
μ /mm ⁻¹	0.108		
F(000)	532.1		
Crystal size/mm ³	0.05 × 0.02 × 0.015		
Radiation	Synchrotron (λ = 0.7)		
2 Θ range for data collection/°	5.12 to 64.74		

Index ranges $-9 \leq h \leq 9, -30 \leq k \leq 30, -12 \leq l \leq 12$
 Reflections collected 22686
 Independent reflections 3909 [Rint = 0.0357, Rsigma = 0.0257]
 Data/restraints/parameters 3909/0/174
 Goodness-of-fit on F2 1.063
 Final R indexes [$I \geq 2\sigma(I)$] R1 = 0.0571, wR2 = 0.1497
 Final R indexes [all data] R1 = 0.0776, wR2 = 0.1637
 Largest diff. peak/hole / e \AA^{-3} 0.62/-0.42

Crystal data and structure refinement for TMB-TCQNF₄ at 150K

Identification code 2097175
 Empirical formula C₂₈H₂₀F₄N₆
 Formula weight 516.505
 Temperature/K 150.0
 Crystal system monoclinic
 Space group P2₁/m
 a/ \AA 6.6095(1) b/ \AA 22.9174(5) c/ \AA 8.3274(2)
 $\alpha/^\circ$ 90 $\beta/^\circ$ 109.247(2) $\gamma/^\circ$ 90
 Volume/ \AA^3 1190.87(5) Z=2
 ρ_{calc} g/cm³ 1.440
 μ/mm^{-1} 0.107
 F(000) 532.1
 Crystal size/mm³ 0.05 \times 0.02 \times 0.015
 Radiation Synchrotron ($\lambda = 0.7$)
 2 θ range for data collection/ $^\circ$ 5.1 to 58.16
 Index ranges $-9 \leq h \leq 9, -30 \leq k \leq 30, -11 \leq l \leq 11$
 Reflections collected 21041
 Independent reflections 3386 [Rint = 0.0317, Rsigma = 0.0258]
 Data/restraints/parameters 3386/0/174
 Goodness-of-fit on F2 1.054
 Final R indexes [$I \geq 2\sigma(I)$] R1 = 0.0509, wR2 = 0.1394
 Final R indexes [all data] R1 = 0.0698, wR2 = 0.1530
 Largest diff. peak/hole / e \AA^{-3} 0.55/-0.33

Crystal data and structure refinement for TMB-TCQNF₄ at 200K

Identification code 2097176
 Empirical formula C₂₈H₂₀F₄N₆
 Formula weight 516.505
 Temperature/K 200
 Crystal system monoclinic
 Space group P2₁/m
 a/ \AA 6.62655(14) b/ \AA 22.8918(4) c/ \AA 8.33673(18)
 $\alpha/^\circ$ 90 $\beta/^\circ$ 109.195(2) $\gamma/^\circ$ 90
 Volume/ \AA^3 1194.32(5) Z=2
 ρ_{calc} g/cm³ 1.436
 μ/mm^{-1} 0.107
 F(000) 532.1
 Crystal size/mm³ 0.05 \times 0.02 \times 0.015
 Radiation synchrotron ($\lambda = 0.7$)
 2 θ range for data collection/ $^\circ$ 5.1 to 64.82
 Index ranges $-9 \leq h \leq 9, -30 \leq k \leq 30, -12 \leq l \leq 12$
 Reflections collected 23086
 Independent reflections 3963 [Rint = 0.0388, Rsigma = 0.0287]
 Data/restraints/parameters 3963/0/174
 Goodness-of-fit on F2 1.090

Final R indexes [$I \geq 2\sigma(I)$] R1 = 0.0690, wR2 = 0.1604
 Final R indexes [all data] R1 = 0.1024, wR2 = 0.1802
 Largest diff. peak/hole / e Å⁻³ 0.52/-0.34

Crystal data and structure refinement for TMB-TCNQF₄ at 300K

Identification code 2097177
 Empirical formula C₂₈H₂₀F₄N₆
 Formula weight 516.505
 Temperature/K 300
 Crystal system monoclinic
 Space group P2₁/m
 a/Å 6.6691(2) b/Å 22.8845(7) c/Å 8.3705(3)
 α/° 90 β/° 108.977(4) γ/° 90
 Volume/Å³ 1208.06(7) Z = 2
 ρ_{calc} g/cm³ 1.420
 μ/mm⁻¹ 0.920
 F(000) 534.0
 Crystal size/mm³ 0.05 × 0.02 × 0.015
 Radiation Cu K_α (λ = 1.54184)
 2θ range for data collection/° 7.72 to 140.12
 Index ranges -8 ≤ h ≤ 7, -26 ≤ k ≤ 27, -10 ≤ l ≤ 10
 Reflections collected 10270
 Independent reflections 2326 [Rint = 0.0955, Rsigma = 0.0834]
 Data/restraints/parameters 2326/0/174
 Goodness-of-fit on F² 1.061

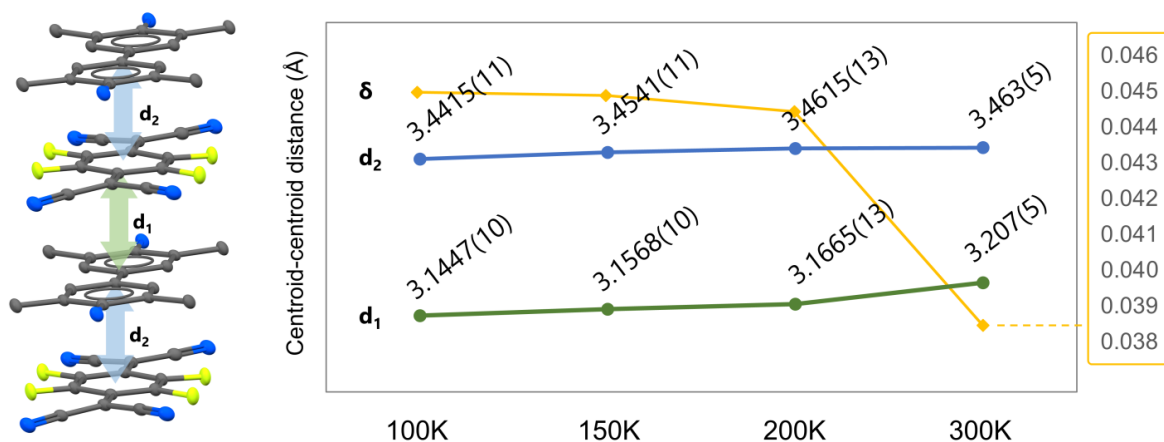


Figure S5. Temperature dependence of intra-dimer (d_1 , green) and inter-dimer (d_2 , blue) distances between the molecular centroids along the a stack axis of TMB-TCNQF₄. The temperature dependence of the dimerization amplitude $\delta = (d_2 - d_1)/(d_2 + d_1)$ is also reported (yellow line).

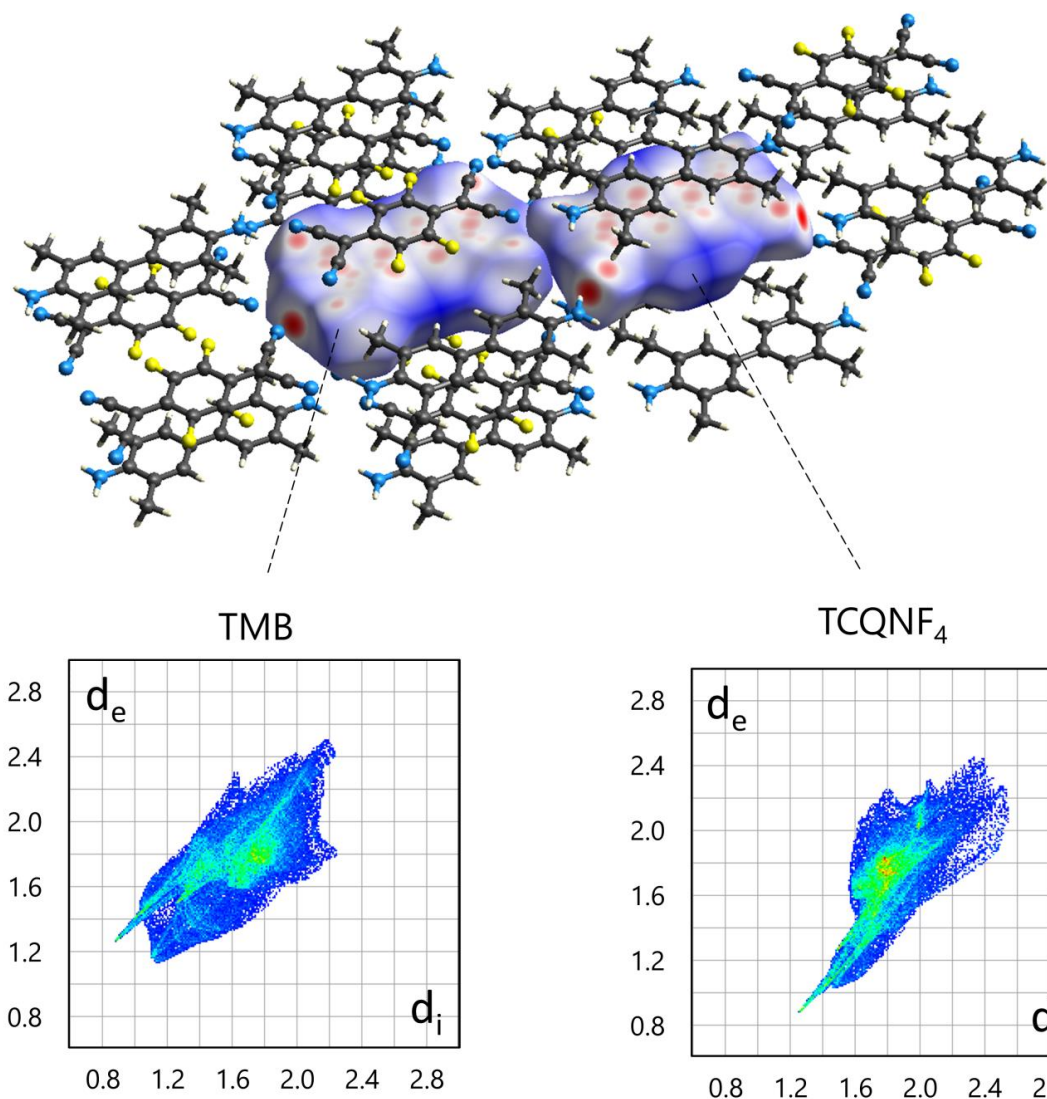


Figure S6. 3D Hirshfeld surfaces and 2D fingerprint plots of TMB-TCNQF₄ at 100 K. Intermolecular contacts are mapped by using a blue-white-red colour scheme, where white marks the Hirshfeld surface regions where the intermolecular atom-atom distances equal the sum of the Van der Waals radii of the involved atoms, red is for regions where the distances are shorter, blue when they are longer. In 2D fingerprint plots, each point represents an individual pair (d_i , d_e), reflecting the distances to the nearest atom inside (d_i) and outside (d_e) of the Hirshfeld d_{norm} surface.

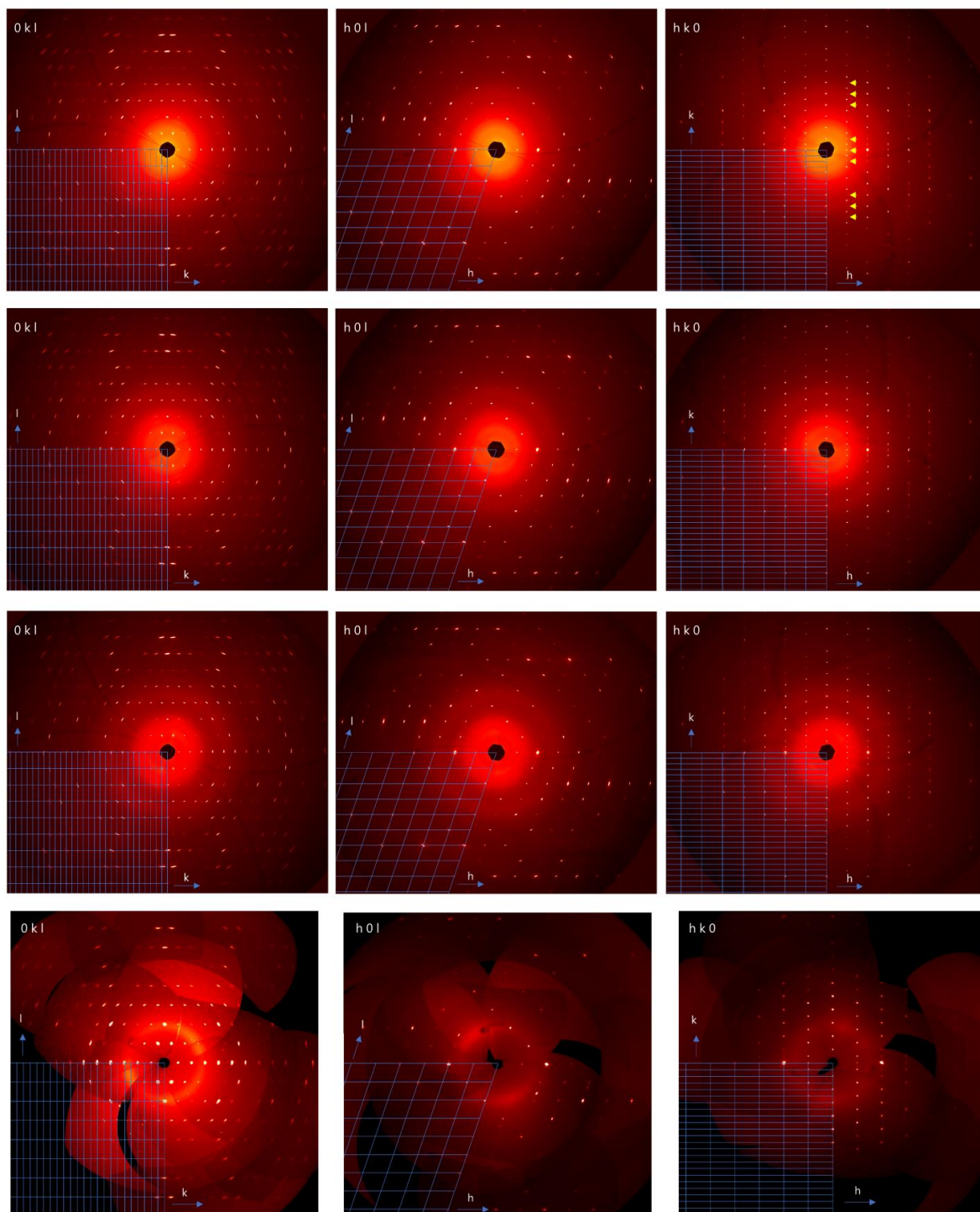


Figure S7. Reciprocal space reconstructions of the main planes of TMB-TCNQF_4 crystals analyzed at 100, 150, 200, and 300 K (from top to bottom, in lines), showing the presence of extra peaks due to the primitive monoclinic $P2_1/m$ lattice. Some of these peaks are highlighted with yellow arrows in the upper right reconstruction.

5. Band structure calculations

Band structure calculations have been performed by the Quantum Espresso package [3], using the PBE USPP pseudopotential pbe-n-rrkjus_psl.

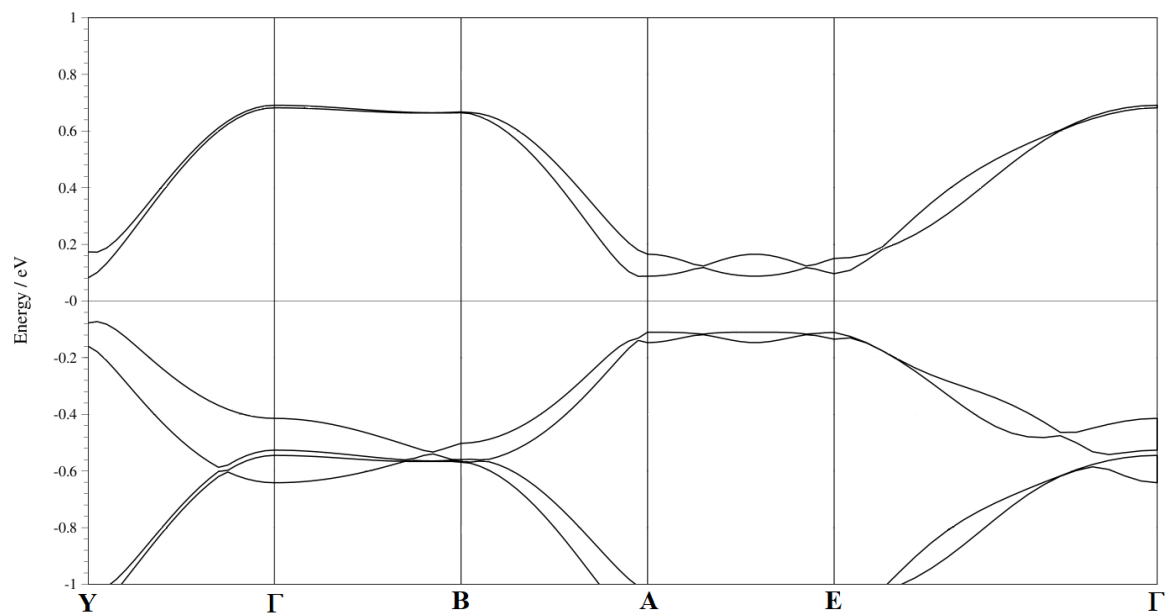


Figure S8. Band structure of TMB-TCNQF₄, $P2_1/m$ crystal structure. $\mathbf{Y}=(0.5,0.0,0.0)$, $\mathbf{B}=(0.0,0.0,0.5)$, $\mathbf{A}=(0.5,0.0,0.5)$, $\mathbf{E}=(0.5,0.5,0.5)$. \mathbf{Y} direction corresponds to stack axis.

6. References

- [1] N. Castagnetti, M. Masino, C. Rizzoli, A. Girlando, and C. Rovira, *Phys. Rev. Materials* **2**, 024602 (2018).
- [2] J. K. H. Fischer, G. D'Avino, M. Masino, F. Mezzadri, P. Lunkenheimer, Z. G. Soos, and A. Girlando, *Phys. Rev. B* **103**, 115104 (2021).
- [3] P. Giannozzi, S. Baroni, N. Bonini, M. Calandra, R. Car, C. Cavazzoni, D. Ceresoli, G. L. Chiarotti, M. Cococcioni, I. Dabo, A. Dal Corso, S. Fabris, G. Fratesi, S. de Gironcoli, R. Gebauer, U. Gerstmann, C. Gougoussis, A. Kokalj, M. Lazzeri, L. Martin-Samos, N. Marzari, F. Mauri, R. Mazzarello, S. Paolini, A. Pasquarello, L. Paulatto, C. Sbraccia, S. Scandolo, G. Sclauzero, A. P. Seitsonen, A. Smogunov, P. Umari, R. M. Wentzcovitch, *J.Phys.:Condens.Matter* **21**, 395502 (2009).
- [4] O.V. Dolomanov, L.J. Bourhis, R.J. Gildea, J.A.K. Howard, H. Puschmann, *J. Appl. Crystallogr.* **42**, 339–341 (2009).
- [5] G. M. Sheldrick, *Acta Cryst. C* **71**, 3-8 (2015).
- [6] P.R. Spackman, M.J. Turner, J.J. McKinnon, S.K. Wolff, D.J. Grimwood, D. Jayatilaka, M.A. Spackman, *J. Appl. Cryst.* **54**, 3 (2021).